Ecological Processes

RESEARCH

Open Access

# Rare earth element geochemistry in soils along arid and semiarid grasslands in northern China

Yi-Wen Cao[1,2], Xiao-Ming Liu[3], Chao Wang[1], Edith Bai[4] and Nanping Wu[5*]

## Abstract

**Background:** Rare earth elements (REE) are a group of trace elements that behave geochemically coherently. REE fractionation patterns normalized to reference materials provide a powerful tool for documenting pedogenesis. In-soil processes are particularly difficult to illustrate with respect to contemporary and past climate conditions. In this study, we characterize the rare earth element (REE) contents in bulk soils and respective geochemical fractions (e.g., exchangeable, carbonate-bound, reducible, and oxidizable fractions) and to decipher the relationships between REE geochemistry components and climatic factors across a large-scale northern China transect (NCT).

**Results:** Across the NCT, bulk REE concentrations ranged from 55.2 to 241.1 μg $g^{-1}$ with a main portion in the residual fraction (49–79%), followed by oxidizable fraction (2–40%), reducible fraction (3–22%), carbonate-bound fraction (0.1–16%), and negligible exchangeable fraction. The REE contents of geochemical components (carbonate-bound, reducible, and oxidizable) in topsoils correlated to climate factors (mean annual precipitation, mean annual temperature, potential evaporation, and aridity index (AI)). The normalized abundances to the upper continental crust (UCC) composition show that the middle REE was generally enriched than the light REE and heavy REE in topsoils along the transect. The overall UCC-normalized bulk REE patterns in topsoils and subsoils were similar, characterized by weak negative Ce anomalies and positive Eu anomalies.

**Conclusions:** Our data in topsoils and depth profiles collectively suggest that cycling of REE was primarily regulated by abiotic processes in area with AI < 0.2, while the biological effect on REE circulation in soil played a more effective role in area with AI > 0.3. The similar UCC normalized patterns in topsoils suggest that the REE was originated from a common source with limited influences from other sources (e.g., atmospheric dusts and anthropogenic contributions). Our results to some extent provide evidence for climatic influence REE distribution patterns both in topsoils and subsoils across the continental-scale transect. Our investigation gives insights into future studies on vertical REE mobility and its associated biogeochemical pathways.

**Keywords:** Rare earth elements, Soil, Grassland, Northern China, Aridity index

## Introduction

The rare earth elements (REEs) are a set of 17 metallic elements as defined by the International Union of Pure and Applied Chemistry (IUPAC), including the lanthanide series elements (La, Ce, Pr, Nd, Pm, Sm, Eu, Gd, Tb, Dy, Ho, Er, Tm, Yb, and Lu) plus yttrium (Y) and scandium (Sc). Despite their names, REEs (with the exception of short-lived radioactive promethium) are abundant and account for ~ 0.015% (w/w) of the Earth's crust. For

*Correspondence: wunp@idsse.ac.cn
[5] Present Address: Institute of Deep-Sea Science and Engineering, Chinese Academy of Sciences, Sanya 572000, China
Full list of author information is available at the end of the article

example, the contents of the lanthanides range from 63 μg $g^{-1}$ in Ce to 0.5 μg $g^{-1}$ in Tm (Tyler 2004). The REEs are widely applied in fertilizers to improve crop yields (Pang et al. 2001), and they are also essential for high-tech industries with an estimated global demand of 1200–1500 kilotons for expanding applications (e.g., Balaram 2019; Humphries 2010; Kumari et al. 2015; Mihajlovic and Rinklebe 2018).

Due to their common electronic structure of progressive filling of 4f orbit, the lanthanide elements (La to Lu) have similar physicochemical characteristics (e.g., ionic radii, $3^+$ valent state and electronegativity) and tend to exist together naturally rather than individually (Migaszewski and Gałuszka 2015; Tyler 2004). However, the lanthanides may be fractionated during different processes and under different environmental conditions. For example, Ce and Eu have variable electronic configuration; therefore, they have $4^+$ valent state and $2^+$ valent state under oxic and reducing redox conditions, respectively. In addition, the lanthanides are usually divided into three groups based on their subtle differences in electronegativity: light REE (LREE, from La to Nd), middle REE (MREE, from Sm to Ho) and heavy REE (HREE, from Er to Lu). The consequences and geochemical signatures of this fine distinction can be magnified and recorded in material circulation of the rock–soil–plant system. Thus, the geochemistry of REEs is widely used to trace parent rock lithology, weathering intensities, and redox changes in soil (e.g., Chapela et al. 2018; Chen et al. 2014; Laveuf and Cornu 2009; Liu et al. 2022; Liu et al. 2021a, b; Vermeire et al. 2016).

The REE contents in soil are principally the weighted average of the REE levels in geochemical components and the abundances of REE-bearing different constitutes. Five components, including exchangeable fraction, carbonate-bound fraction (highly mobile and bioavailable), Fe/Mn oxyhydroxide-affinity fraction (reducible), organic matter/sulfide-adsorption fraction (oxidizable) and the residue fraction in minerals (less mobility and non-bioavailable) can be operationally extracted and separated to show different forms of REE (e.g., Hu et al. 2006; Laveuf et al. 2012; Mihajlovic et al. 2014). Changes in environmental factors and edaphic factors such as temperatures, salinity, pH, and redox conditions have been documented to influence the REE redistribution and mobility into different geochemical components (Andrade et al. 2022; Cao et al. 2001; Davranche et al. 2011; Guénet et al. 2018; Pourret et al. 2007; Tyler, 2004). For instance, the releases of REE from Fe/Mn oxyhydroxide were found to enhance with increasing pH and decreasing redox potential in soils (e.g., Cao et al. 2001). However, the influence of long-range climatic factors on the distribution and mobility of soil REE on a continental scale is still unclear. Here, we address two important questions: (1) How would different REE geochemical fractions in soil vary along an aridity gradient? And (2) What biogeochemical and ecological information might those variations provide?

The northern China transect (NCT) is a 3700 km West–East grassland transect from Xinjiang to Inner Mongolia in northern China. The ecosystem types along the NCT shift from the typical steppe and meadow steppe from west to east, an ideal region to investigate elemental biogeochemistry along large-scale climatic gradients (e.g., Wang et al. 2014; Feng et al. 2016; Luo et al. 2016a, b). Previous studies have shown that cycling of nitrogen, phosphorus, sulfur, and carbon could be loosely decoupled and tightly coupled across this transect, shifting from geochemical to biological control on the nutrient elemental cycling over a narrowly defined aridity index (AI, the ratio of precipitation to potential evapotranspiration) threshold (AI = 0.20 to 0.30, Wang et al. 2014; Feng et al. 2016; Luo et al. 2016a, b).

REE contents and their mobility in soils are linked to weathering intensity of parent materials, the storage capacity of authigenic soil phases (e. g. carbonates, secondary oxide and oxyhydroxide, kaolinite and smectite and organic ligands) and the fluctuations of redox conditions. As all above mentioned factors are affected by climatic parameters (such as temperatures and precipitations), it is reasonable to hypothesize that the REE mobilization, redistribution, and fractionation will be impacted by climate change. The aims of this study are to (1) quantify the abundances and geochemical fractions of REE in surface soils; (2) examine the relationships between REE abundances and climate factors/edaphic factors and explore their implications; (3) compare the difference of REE distribution in the depth profiles to understand their potential vertical mobility.

## Materials and methods

### Study sites

A total of 21 study sites were selected along the northern China transect (NCT, Fig. 1). The NCT locates in the mid-latitude temperate region, spanning from the arid to semi-arid continental climate, and the representative types of vegetation are alpine meadow, desert steppe, typical steppe and meadow steppe from west to east. The terrains along the transect are generally flat with tablelands and gently rolling hills (Luo et al. 2016b), a unique feature that allows to deconvolve the climate effects from the minor/diminished topography effects in pristine soils at or near steady state with respect to elemental cycling along a well-constrained climate gradient.

Mean annual precipitation (MAP) ranges from 34 to 406 mm along the NCT, with > 77% of rainfall occurring

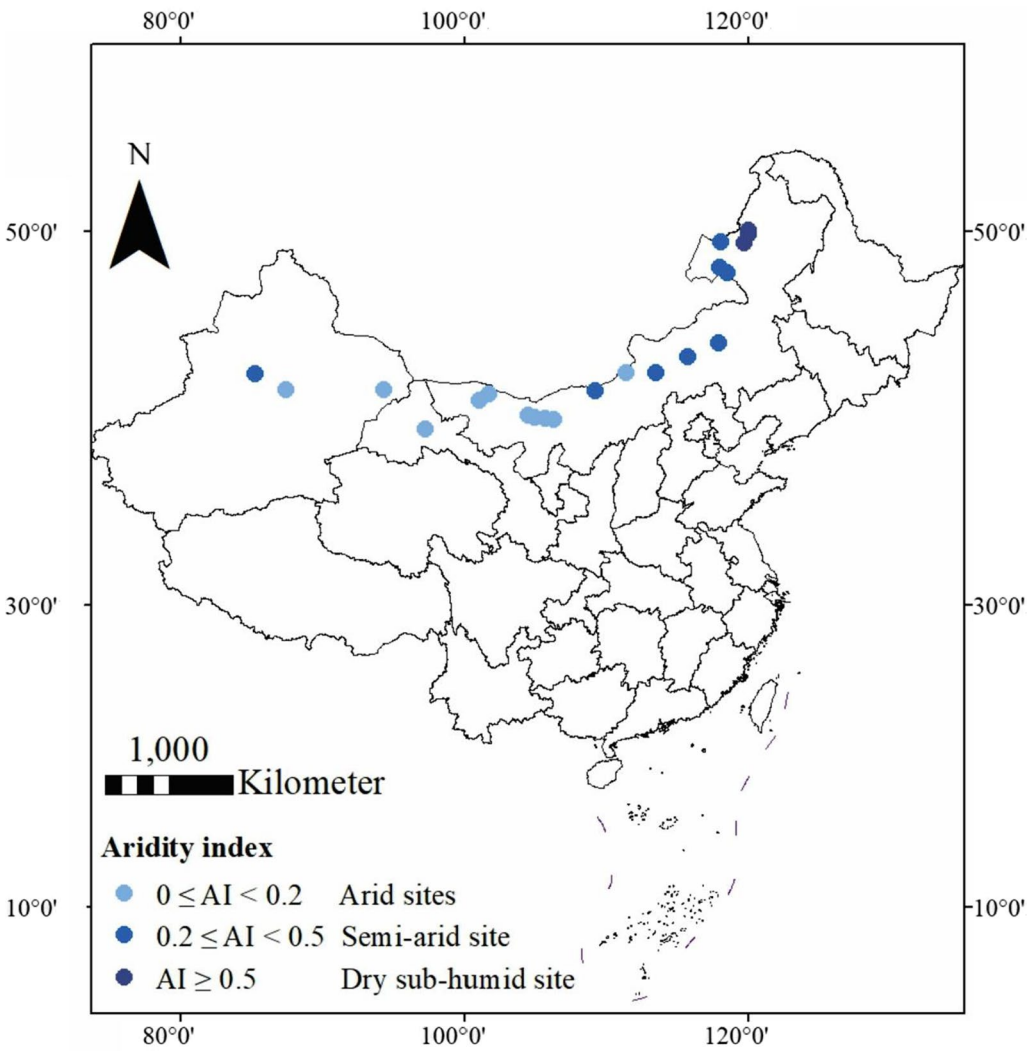


**Fig. 1** Map of sampling localities on a continental scale. Across northern China from west to east, the sampling sites are labeled S01–S21 in order. Based on the aridity index (AI), the sites are divided into three climate subtypes: arid areas ($0 \leq AI < 0.2$, represented by light blue circles), semi-arid areas ($0.2 < AI \leq 0.5$, represented by blue circles), and dry sub-humid areas ($AI \geq 0.5$), represented by dark blue circles)

during June–September. The annual air temperature (MAT) ranges from − 3 °C to 10 °C from west to east. During November–March, the average monthly temperatures are below 0 °C at all sites, while the highest average monthly temperatures are 15–25 °C during June–August. The annual potential evapotranspiration (PET), a complex function of MAT, varies from 611 mm at the western sites to 1202 mm at the eastern sites (Wang et al. 2014). An overall negative correlation between annual MATs and annual MAPs exists among the sites along the transect (Feng et al. 2016). In this study, we use an integrated parameter of aridity index (AI = MAP/PET) to reflect the climate variability and change. Accordingly, the studied NCT region is divided into three subtypes, including hyper-arid and arid ($0 \leq AI < 0.2$), semi-arid ($0.2 \leq AI < 0.5$) and dry sub-humid ($AI \geq 0.5$) (Middleton and Thomas 1997). Specifically, the studied sites (S02, S03, S04, S05, S06, S07, S08, S09, S10) are in the arid area, and other sites are in the semi-arid (S01, S12, S13, S14, S15, S16, S17, S18) and dry sub-humid areas (S19, S20, S21).

The soil is classified into three types: Haplic Calcisols (S01–S08), Calcic Cambisols (S09–S12), and Calcic Kastanozems (S13–S21) (Feng et al. 2016). The Haplic Calcisols represents an initial stage of soil formation with significant accumulation of secondary calcium carbonate; Calcic Cambisols have minimal B-horizon development, and are considered to be in an intermediate stage

of development; Kastanozems has a deep, dark-colored surface horizon with an accumulation of organic matter, and an accumulation of calcium carbonate within 100 cm of the soil surface (FAO 1993, 2014).

Soil sampling was conducted in regions far away from the road to minimize anthropogenic interference. For each site, two 50× 50 m plots were selected and divided into five 1 × 1 m subplots in each corner and center. In each subplot, twenty random soil samples were collected from 0 to 10 cm below the surface (topsoils). According to the climate subtypes and locations, we also selected four representative sites (S03, S09, S13, S19) to study vertical REE geochemical behavior. For sites S03, S09, S13, and S19, soil samples from the underlying soil (10–20, 20–40, 40–60, and 60–100 cm) were collected.

#### Sequential extraction procedure and chemical analysis

Soil samples were first passed through a 2-mm polyethylene sieve to remove rocks and plant residue in situ. The air-dried soil samples were then ground into a fine powder in the laboratory and fully mixed and homogenized to be used as a representative sample. Soil pH values, clay contents, total organic carbon concentrations were determined by Wang et al. (2014), and were briefly described below. The soil pH value was determined in a soil–water ratio of 1:2.5 using the pH electrode. The soil organic carbon (SOC) concentrations were measured using an elemental analyzer (2400II CHN elemental analyzer; Perkin–Elmer, USA) at the Stable Isotope Facility of the University of California, Davis after removing carbonates using HCl (0.5 M) (Wang et al. 2014). The total inorganic carbon was measured by measuring the volume of $CO_2$ released from air-dried soil with HCl (2 M) at room temperature (Luo et al. 2016a).

A BCR sequential extraction procedure modified from Li et al. (2020) was also used to extract the geochemical components of REE and the general protocol was briefly described below (also see the flowchart of REE extraction protocol in Additional file 1: Fig. S1):

- Step 1: approximately 500 mg soil was weighed in a polypropylene centrifuge tube and 25 ml 0.05 M $CaCl_2$ solution was added to the tube. The tube was then shaken for 8 h at ambient temperature (22–23 °C), and centrifuged to obtain the residue and supernatant;
- Step 2: 20 ml 0.11 mol $L^{-1}$ acetic acid solution was added to the residue from step 1, and shaken for 16 h, and extracts retained as in step 1;
- Step 3: residues from step 2 mixed with 20 ml 0.5 mol $L^{-1}$ hydroxylamine hydrochloride (pH = 2) and shaken for 16 h at ambient temperature (22–23 °C). The extracts retained as in step 2;
- Step 4: residues from step 3 reacted with 5 ml 30% $H_2O_2$ for 1 h at ambient conditions (22–23 °C). The mixtures were evaporated (repeated twice). 25 ml 1 mol $L^{-1}$ pH = 2 $CH_3COONH_4$ solution was then added to the dried residues, and shaken for 16 h at ambient temperature (22–23 °C).
- Step 5: residues from step 4 were digested with HF–$HNO_3$–HCl solution in closed Teflon™ beakers for 3 days (Li et al. 2019).

According to the BCR sequential extraction method (Mittermüller et al. 2016; Rauret et al. 1999), the supernatants of step 1, step 2, step 3, and step 4 are exchangeable fraction, carbonate-bound fraction, reducible fraction, and oxidizable fraction, respectively. The bulk REE contents were calculated as the sum of geochemical fractions extracts. REE chemical extraction was conducted at the laboratory of deep-sea geobiology, Institute of Deep-Sea Science and Engineering, Chinese Academy of Sciences (IDSSE-CAS). The contents of reducible Fe, Mn and REE were determined using an inductively coupled plasma-mass spectrometry (Thermo Fisher Scientific ™ iCAP ™ RQ ICP-MS) at the analytical center of IDSSE–CAS. Internal standards, including Be, Ge, Rh, and Ir in 2% $HNO_3$, were used to correct instrumental drifts. The calibration standard (BCR667 and GBW07986) and blank samples were inserted every 20 samples and were routinely analyzed to evaluate the analytical accuracy and precision. The external relative precisions associated with bulk REE measurements of BCR667 and GBW07986 were 4.2 and 2.5%, respectively.

The mineralogical compositions of soils are deduced from by X-ray diffractogram. The general procedure of X-ray diffraction analysis is briefly described as follows: First, the air-dried soil sample was ground into a fine powder by an agate mortar and pestle and passed through a 200 mesh sieve. Then the powders were determined by X-ray diffractometry (XRD) (Ultima IV, Rigaku, Japan) with Cu Ka radiation (40 kV and 40 mA) at a scanning rate of 1 $min^{-1}$ and 0.02° step size at the Institute of Soil Science, Chinese Academy of Sciences.

#### Statistical analysis

Pearson's correlation analyses were applied to study the relationships between rare earth elements (bulk and geochemical components) and climate factors as well as soil properties. The strength of the association between the variates was evaluated by $P$ values: $P < 0.05$, representing the correlation is significant at 95% confidence interval, $P < 0.01$, representing the correlation is significant at 99% confidence interval. The statistical analysis was done using the software of PASW Statistics 18.

## Results

### Geochemical characteristics of REE in topsoils

Bulk REE contents in topsoils (0–10 cm) along the NCT varied significantly from 55.2 μg $g^{-1}$ at S04 to 241.1 μg $g^{-1}$ at S02 with an average value of 118.3 ± 36.8 μg $g^{-1}$ (SD) (Additional file 2: Table S1). The exchangeable fractions at all sites were practically negligible. The most mobile and bioavailable REE (15.3–79.0 μg $g^{-1}$), including carbonate-bound, reducible, and oxidizable fractions, accounted for 21–51% of the bulk REE contents among all sites (Fig. 2a) and had a wide range of values from 0.1 to 12.0 μg $g^{-1}$, from 5.6 to 31.3 μg $g^{-1}$, and from 1.5 to 63.0 μg $g^{-1}$, respectively (Additional file 2: Table S3). At the arid sites of S02, S03, S04, S05, S06, S07, S08, S09, S10, the carbonate-bound fractions (3.5 to 12.0 μg $g^{-1}$) were generally higher than those at other sites (Additional file 2: Table S3). The absolute amounts of reducible REE contents had no obvious difference among all the sites, but the relative fractions of these geochemical components were generally higher at arid sites (Fig. 2a). The oxidizable fractions (9.3 to 63.0 μg $g^{-1}$) dominated over the reducible fractions (5.6 to 16.1 μg $g^{-1}$) at the sites of S1, S14, S15, S16, S17, S18, S19, S20, S21.

The REE concentrations are usually normalized relative to the upper continental crust (UCC, refer to Taylor et al. 1981) to eliminate the "even–odd" effect and show the distribution patterns of individual REE (Vermeire et al. 2016). The normalization and parameters defined

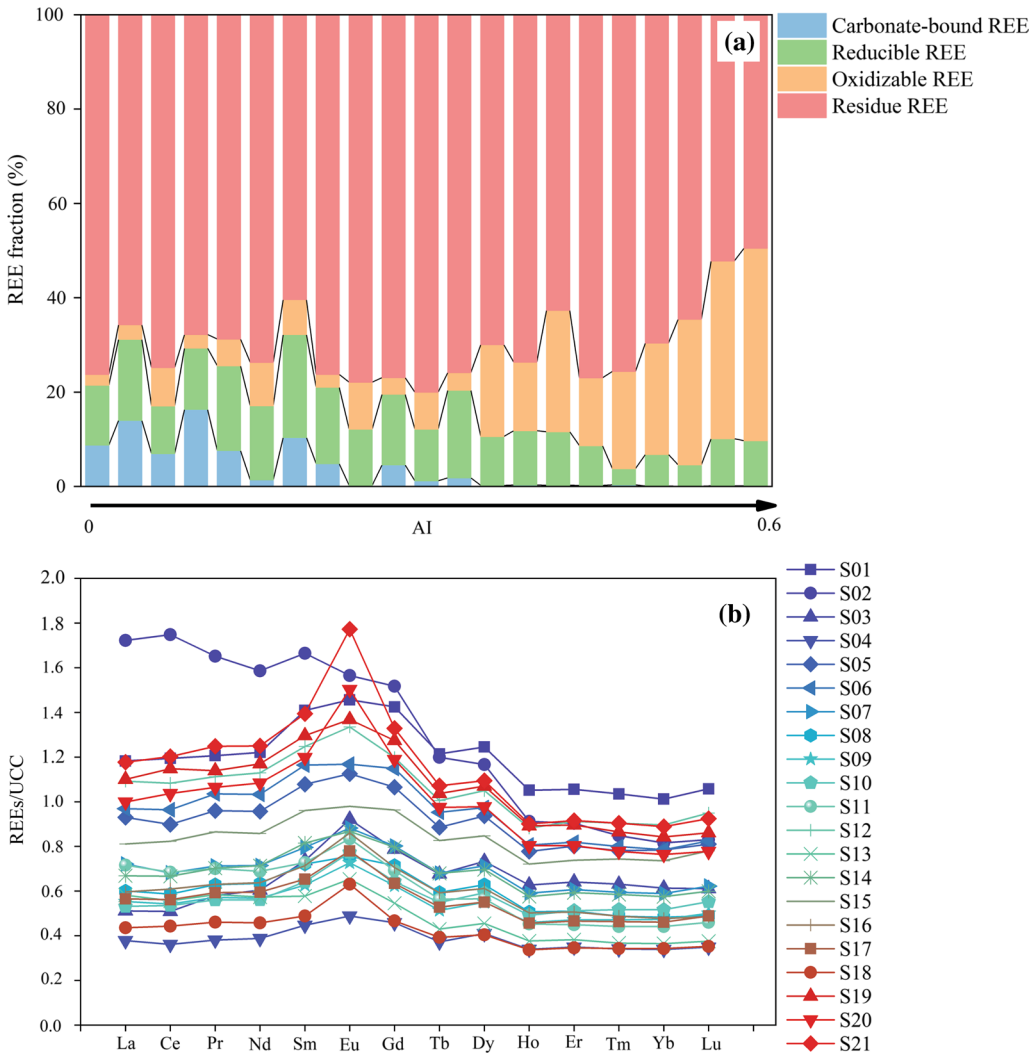


**Fig. 2** **a** Relative geochemical fractions (carbonate-bound, reducible, oxidizable and residue) of rare earth elements (REE) vs. aridity index (AI) in topsoils (0–10 cm). **b** Upper continental crust (UCC) normalized patterns of bulk REE in topsoils (0–10 cm) along the northern China transect (S01–S21)

below facilitate comparisons of REE patterns graphically between sites. $La_N/Yb_N$ ratios, $La_N/Gd_N$ ratios, and $Gd_N/Yb_N$ ratios are represented as the fractionations of LREE to HREE, LREE to MREE, and MREE to HREE, respectively (Brito et al. 2021). The Ce and Eu anomalies are defined as $Ce/Ce^* = Ce_N/(La_N \times Pr_N)^{0.5}$ and $Eu/Eu^* = Eu_N/(Sm_N \times Gd_N)^{0.5}$, respectively. The subscript N in the parameters above denotes REE concentrations normalized against UCC (Liu et al. 2019; Taylor and McLennan 1985).

UCC-normalized bulk REE patterns (Fig. 2b) were generally similar, characterized by MREE enrichment relative to LREE and HREE ($La_N/Gd_N = 0.6–1.1$, $Gd_N/Yb_N = 1.2–1.9$), weak negative Ce anomalies ($Ce/Ce^* = 0.9–1.0$) and positive Eu anomalies ($Eu/Eu^* = 1.0–1.3$) (Additional file 2: Table S1). In contrast, UCC-normalized REE patterns of geochemical fractions showed distinguished features (Fig. 3, Additional file 2: Table S4): (1) the carbonate-bound fraction was characterized by HREE depletion ($La_N/Yb_N = 1.2–4.5$, $Gd_N/Yb_N = 1.9–3.8$), pronounced negative Ce anomalies ($Ce/Ce^* = 0.3–0.9$) and positive Eu anomalies ($Eu/Eu^* = 1.0–1.9$), except for small Eu anomaly of 0.9 at site S02); (2) the reducible fractions generally showed HREE depletions ($La_N/Yb_N = 0.8–3.1$, $Gd_N/Yb_N = 1.7–2.4$) and negative Eu anomalies ($Eu/Eu^* = 0.6–1.0$, except for the site S08 with a small positive Eu anomaly of 1.1); (3) the oxidizable fractions revealed clear MREE enrichments ($La_N/Gd_N = 0.3–1.7$, $Gd_N/Yb_N = 1.2–2.1$), and moderate Eu anomalies ($Eu/Eu^* = 0.7–1.2$); and (4) the patterns of residue fractions were characterized by HREE depletion ($La_N/Yb_N = 0.7–2.0$, $Gd_N/Yb_N = 1.1–1.9$), with positive Eu anomalies ($Eu/Eu^* = 1.0–1.6$).

### Geochemical characteristics of REE in depth profiles at selected sites

The depth-profile REE patterns showed site-specific variations in carbonate-bound, reducible and oxidizable fractions, but with dominant residue fractions (Fig. 4, Additional file 2: Table S5, 63.1–94.5 μg $g^{-1}$ at S03,

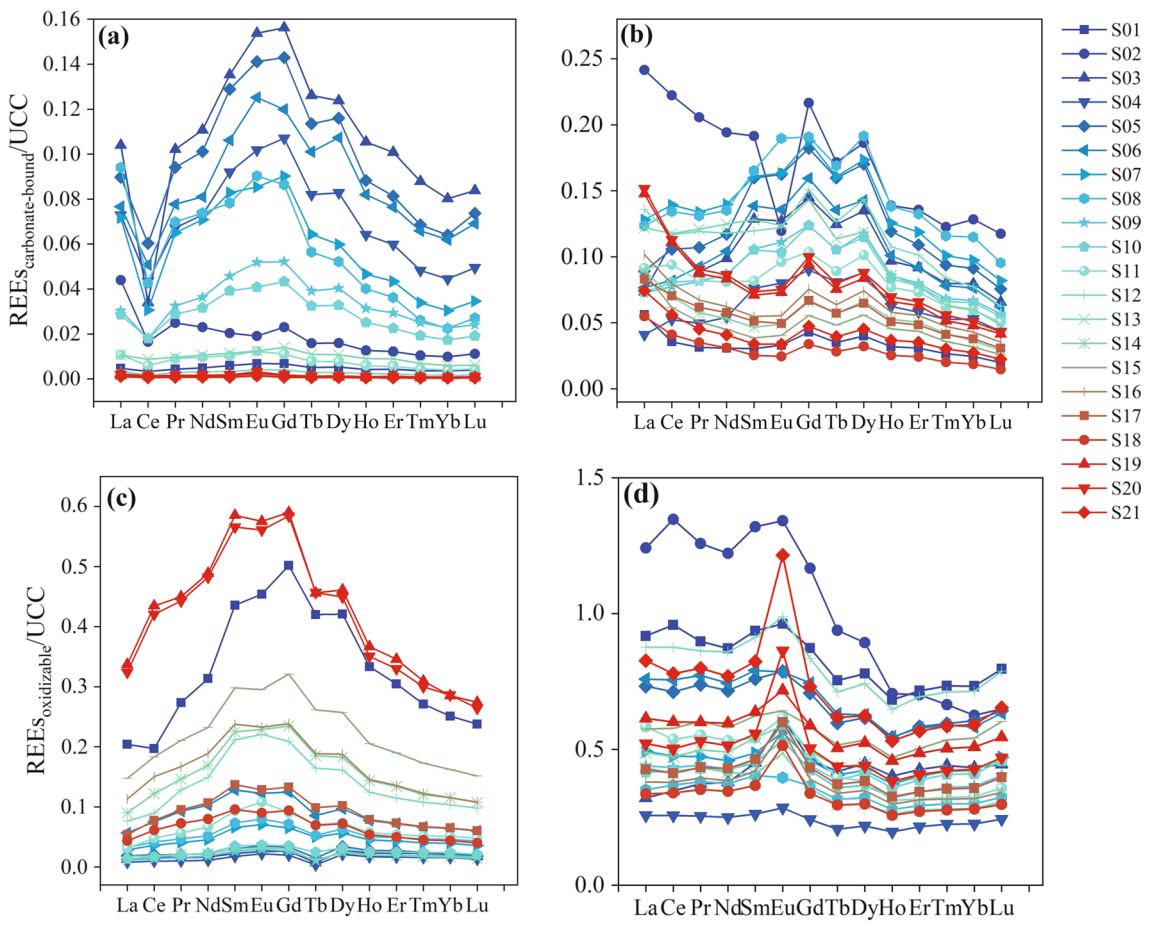


**Fig. 3** Upper continental crust (UCC) normalized patterns of **a** carbonate-bound REE, **b** reducible REE, **c** oxidizable REE, and **d** residue REE in topsoils (0–10 cm) along the northern China transect

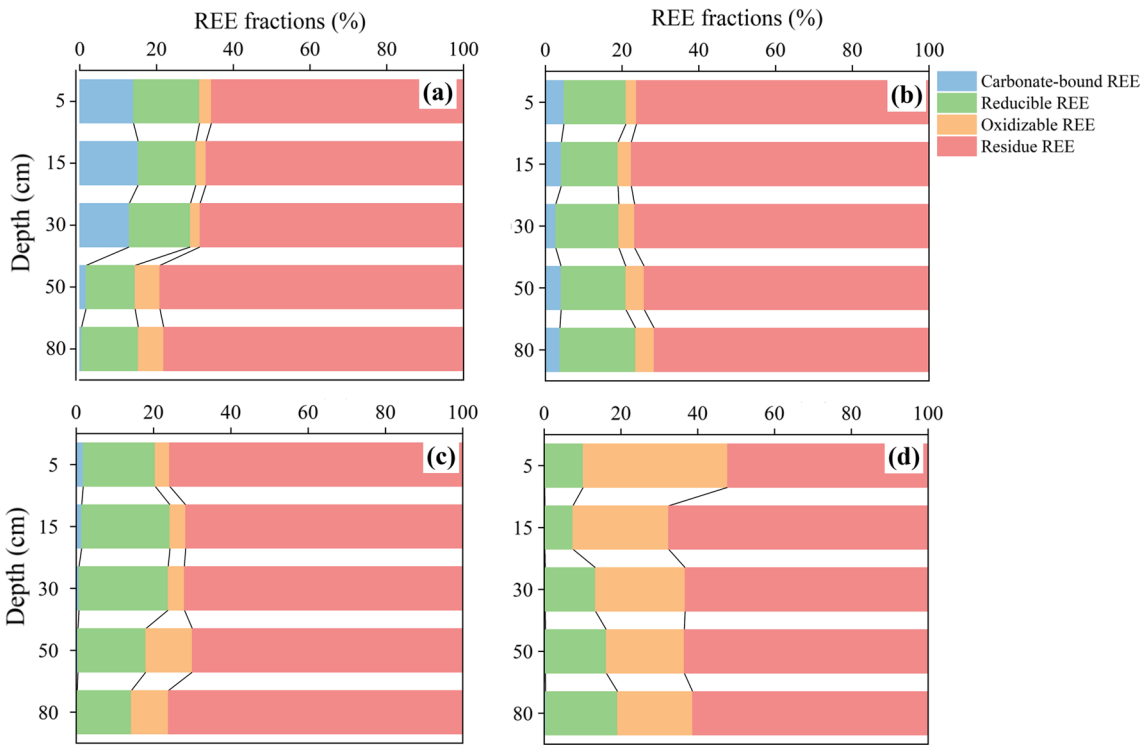


**Fig. 4** Depth profiles (0–10, 10–20, 20–40, 40–60, and 60–100 cm) of relative geochemical fractions in soil at selected study sites. **a** S03, aridity index (AI) = 0.03, **b** S09, AI = 0.10, **c** S13, AI = 0.22, **d** S19, AI = 0.51)

81.0–110.1 μg $g^{-1}$ at S09, 76.1–122.3 μg $g^{-1}$ at S13, and 85.1–166.5 μg $g^{-1}$ at S19). In the arid site S03, carbonate-bound fractions in upper soil (13–15% in the layers of 0–10, 10–20, and 20–40 cm) were significantly higher than that in deep soil (0.4–2% in the layers of 40–60 and 60–100 cm), while the reducible and oxidizable fractions varied over a small range in the depth (13–17 and 2–7%, respectively). At the semi-arid site S09, the carbonate-bound, reducible and oxidizable fractions did not show noticeable depth changes, varying within 3–5, 15–20, and 3–6%, respectively. At the semi-arid site S13, the variations in carbonate-bound, reducible and oxidizable fractions were also within small fluctuations (0.2–2, 14–22 and 3–8%, respectively). At the dry sub-humid site S19, the carbonate-bound fractions were extremely low (0.1–0.3%), while the reducible fractions generally increased with depth (7–18%) and the oxidizable fractions decreased with the depth (18–40%).

The UCC-normalized patterns for bulk REE and geochemical fractions of selected sites also showed various characteristics with depth (Fig. 5, Additional file 2: Table S5 and S7). However, the overall patterns of bulk REE were similar in topsoils and subsoils at all sites, showing HREE depletions ($La_N/Yb_N$ = 0.8–1.6, $Gd_N/Yb_N$ = 1.0–1.5), positive Eu anomalies (Eu/Eu* = 1.1–1.5).

### Correlations among REE geochemical fractions, climatic factors and soil properties

Across all sites, the carbonate-bound fractions were negatively correlated with aridity index (AI) (Table 1, $r = -0.81$, $P < 0.01$) and mean annual precipitation (MAP) (Table 1, $r = -0.85$, $P < 0.01$), but positively correlated with mean annual temperature (MAT) (Table 1, $r = 0.83$, $P < 0.01$) and potential evapotranspiration (PET) (Table 1, $r = 0.86$, $P < 0.01$). The reducible fractions had no correlations with AI and MAP, but had but had positive correlations with MAT (Table 1, $r = 0.48$, $P < 0.01$) and PET (Table 1, $r = 0.46$, $P < 0.01$). In contrast, the oxidizable fractions showed positive correlations with AI (Table 1, $r = 0.81$, $P < 0.01$) and MAP (Table 1, $r = 0.77$, $P < 0.01$), and negative correlations with MAT (Table 1, $r = -0.71$, $P < 0.01$) and PET (Table 1, $r = -0.68$, $P < 0.01$).

There were no discernible relationships between carbonate-bound REE concentrations and total Fe–Mn abundances and clay contents (Table 1). There were positive correlations between carbonate-bound fractions and pH values (Table 1, $r = 0.52$, $P < 0.05$), total inorganic carbon (TIC) concentrations (Table 1, $r = 0.46$, $P < 0.05$), and the negatively correlation with total organic carbon (TOC) (Table 1, $r = -0.58$, $P < 0.01$). The reducible fractions were only positively

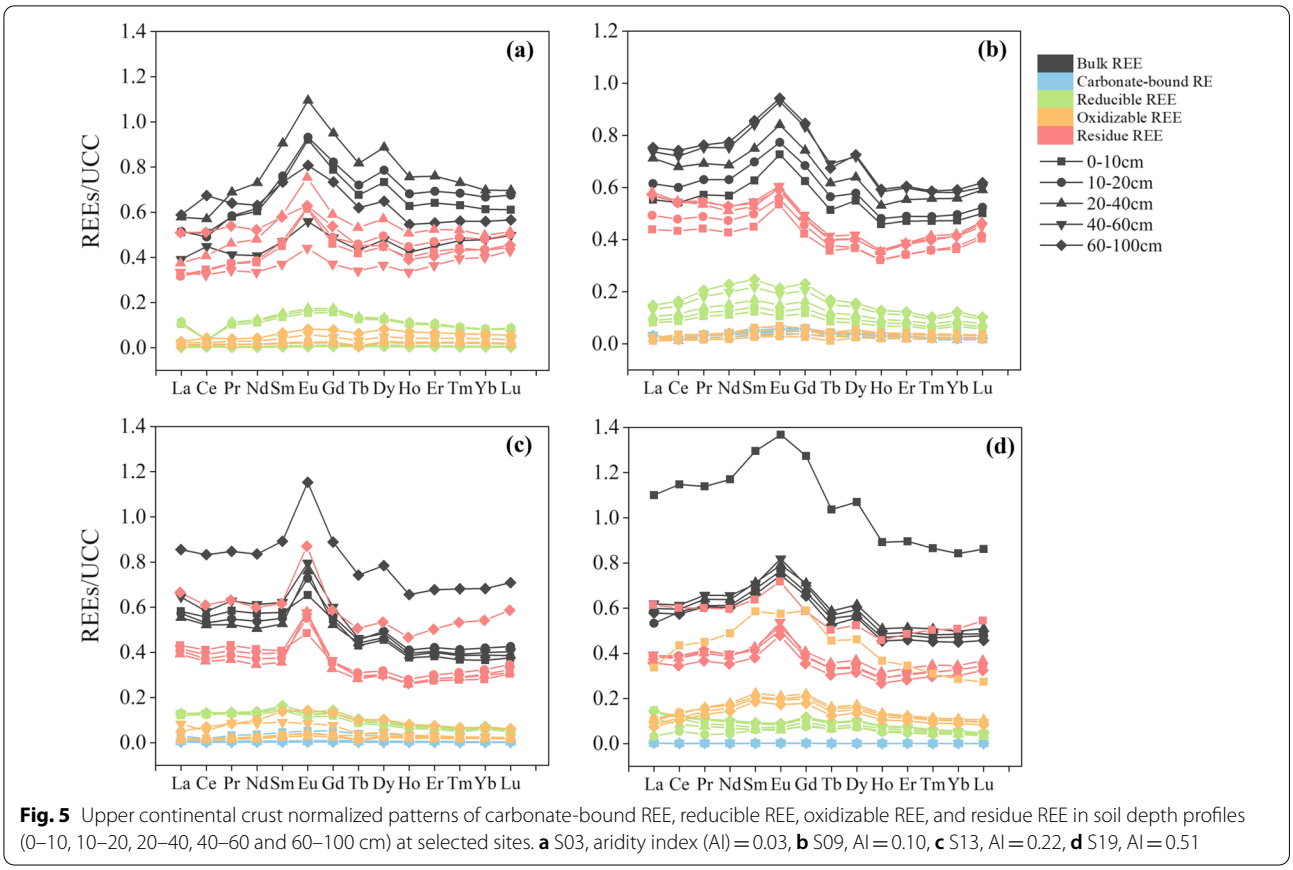


**Fig. 5** Upper continental crust normalized patterns of carbonate-bound REE, reducible REE, oxidizable REE, and residue REE in soil depth profiles (0–10, 10–20, 20–40, 40–60 and 60–100 cm) at selected sites. **a** S03, aridity index (AI) = 0.03, **b** S09, AI = 0.10, **c** S13, AI = 0.22, **d** S19, AI = 0.51

**Table 1** Pearson correlation coefficients between climate factors and soil properties with REE concentrations (μg $g^{-1}$) of bulk and geochemical fractions in topsoils (0–10 cm) along the transect. Locations of the sites (S01–S21) are plotted in Fig. 1

| | AI | MAT | MAP | PET | pH | TOC | Clay | R Fe–Mn | TIC |
|---|---|---|---|---|---|---|---|---|---|
| Bulk | ns | ns | ns | ns | ns | ns | ns | ns | ns |
| Carbonate-bound | − 0.81** | 0.83** | − 0.85** | 0.86** | 0.52* | − 0.58** | ns | ns | 0.46* |
| Reducible | ns | 0.48* | ns | 0.46* | 0.45* | ns | ns | ns | ns |
| Oxidizable | 0.81** | − 0.71** | 0.77** | − 0.68** | − 0.62** | 0.89** | 0.71** | 0.57** | ns |
| Residue | ns | ns | ns | ns | ns | ns | ns | ns | ns |

*AI* aridity index (unitless), *MAT* mean annual temperature (mm), *MAP* mean annual precipitation (mm), *PET* potential evapotranspiration (mm), *pH* pH value (unitless), *TOC* total organic carbon concentration (mg $g^{-1}$), *Clay* clay fraction (%), *RFe–Mn* the sum of reducible manganese concentration and iron concentration (μg $g^{-1}$), *TIC* total inorganic carbon concentration (μg $g^{-1}$). **$P < 0.01$; *$P < 0.05$, *ns* non-significant correlation at 95 and 99% CI

correlated with pH values (Table 1, $r = 0.45$, $P < 0.05$). The oxidizable fractions presented no evident relationship with TIC but had a positive relationship with total organic carbon concentrations (Table 1, $r = 0.89$, $P < 0.01$), reducible Fe–Mn concentrations (Table 1, $r = 0.57$, $P < 0.01$) and clay contents (Table 1, $r = 0.71$, $P < 0.01$), and presented a negative correlation with pH (Table 1, $r = -0.62$, $P < 0.01$).

## Discussion

Overall, our bulk REE data (55.2 to 241.1 μg $g^{-1}$) in topsoils (0–10 cm) along the NCT were well within the range of the reported Chinese surface soil REE contents (79.5 to 354 μg $g^{-1}$, Cao et al. 2000; Chen and Yang 2010; Liu et al. 2021a, b; Miao et al. 2008), except for a few samples with lower abundances. The general similarity of normalized bulk REE patterns in topsoils and depth profiles at selected sites (Figs. 2b and 5) suggests that

the soil REE source along the NCT was originally from a source with the same lithology. Our normalized bulk REE patterns and bulk REE parameters were significantly different from those seen in Asian dust (e.g., from Taklamakan desert, Qaidam basin, Tengger desert, Indian Thar desert, Loess, and Tibetan Plateau), which have distinguished features of LREE depletion and negative Eu and Ce anomalies (Ferrat et al. 2011). It is reasonable to expect somehow significant influence of atmospheric dust inputs on REE behavior in the surface soils. However, the consistent continental-scale REE patterns across the NCT strongly suggest that the studied soils across the NCT may weather from similar parent rocks and did not acquire other significant sources (e.g., anthropogenic or natural contributions). This provides context for understanding the fate of REE in soil along the NCT. In the following sections, we first discuss the general REE behaviors in the topsoils. Next, we discuss REE contents and normalized patterns of different geochemical fractions. Finally, we briefly explore the implications of REE exchange in the soil depth profiles.

#### REE behaviors of geochemical fractions in topsoils

Our data indicated that the residue fraction comprises the majority of bulk REE (49–79%) at all sampling sites (Fig. 2a). This finding is comparable with earlier results of different soil types reported by Davranche et al. (2011), Mihajlovicet al. (2014), and Sukitprapanon et al. (2019) (e.g., 78% in wetland soil, 45–63% in marsh soil, and 60–90% in agricultural land). It is generally thought that this fraction is fixed in the lattices of minerals and/or strongly adsorbed onto clay minerals, and is not biologically available (Hu et al. 2006). The residue fractions had no relationship with soil properties or climatic factors (Table 1), suggesting that REE contents of residue fractions mainly inherit from parent materials in place.

As shown in Fig. 2a, the carbonate-bound fractions accounted for 0.1–16% of the bulk REE in surface soil. The carbonate-bound fractions in arid sites (AI < 0.2) were generally higher than those in other sites of this study, in soils of mining area in southern China, and of agricultural land and forest belt in Russia (2–3%) ( Liu et al. 2021a, b; Shatrova et al. 2021). Studies have shown that REE can be adsorbed on the surface of carbonate minerals due to electrostatic attraction, but mostly exist in the lattice by replacing $Ca^{2+}$ ions during secondary carbonate formation (Polyakov and Nearing 2003). High evapotranspiration conditions were suggested to facilitate the formation of evaporated minerals including carbonates and upward transfer of soluble REE from deeper soil to the surface (Khorasanipour and Jafari 2018). Therefore, the arid environments (AI < 0.2) may favor higher REE retention by enhanced REE incorporation into carbonates in surface soil. The observed strong positive or negative correlations between carbonate-bound fractions and climate factors ($P < 0.01$, AI, MAP, MAT and PET, Table 1) in our data set are likely explained by the proposed mechanism above.

The reducible fraction is generally adsorbed on amorphous Fe–Mn (hydro)oxides and amorphous Fe sulfides (Cao et al. 2001; Rankin and Childs 1976). This fraction is not usually available for plants unless under reducing conditions (Šmuc et al. 2012). The percentages of this fraction ranged from 3 to 22% with an average of 12%, much smaller than values found in soil that had similar Fe and Mn abundances (Mihajlovic et al. 2019) and in Bohai Bay of China (Zhang and Gao, 2015). A positive correlation between soil pH and reducible REE contents was also observed ($P < 0.05$, Table 1). This might be due to pH-dependent adsorption and desorption kinetics that controls the budget of this fraction of REE, as well as the stability of Fe–Mn (hydro)oxides and sulfides. More interestingly, the reducible fraction does not show an expected positive correlation with the total Fe–Mn concentration. There are two possibilities to explain this observation: (1) part of REE could be adsorbed on the negative surface of organic matter, and they are released under the reducing condition (Davranche et al. 2011; Du Laing et al. 2009); (2) Fe–Mn (hydro)oxides are preferentially embedded into the organic matter matrix, forming the OM–metal nanoparticles that are difficult to be attacked to release REE under the reducing condition (Davranche et al. 2011; Pédrot et al. 2015), which is part of the reason a positive correlation between oxidizable fractions and Fe–Mn contents was observed.

The oxidizable fractions are those complex, absorb, and/or chelate with various forms of organics and sulfides (Mihajlovic and Rinklebe 2018). This component is usually considered to be associated with stable high-molecular-weight organic carbon. Thus it is less mobile and available compared with the carbonate-bound and reducible fractions (Filgueiras et al. 2002; García-Miragaya and Sosa 1994). Strong positive correlations between the oxidizable fractions and total organic carbon concentrations in soil were observed ($P < 0.01$), suggesting that organic matter is a major sink for REE as documented in numerous studies (Brito et al. 2021; Mihajlovic et al. 2014). We found that climate factors and the oxidizable fractions are correlated, showing strong positive correlations with AI and MAP ($P < 0.01$), but negatively correlations with PET and MAT ($P < 0.01$). This observation can be explained by the climatic-controlled preservation and decomposition of organic matter. At sites with higher MAP and AI, soil organic matter preservation is likely greater,

thus leading to higher REE adsorption and less mobility. In contrast, higher PET and MAT may promote rates of organic matter decomposition and enhance REE cycling into other geochemical components and/or lost to the soil system.

As discussed above, the fractions of carbonate-bound and reducible REEs are bound to inorganic minerals, such as secondary carbonates and Fe/Mn oxides, whose formation and stability are primarily controlled by geochemically abiotic processes. The fraction of oxidizable REE is mostly associated with organic carbon, whose formation and stability are mainly controlled by biologic processes. The ratios were less than 1 at the sites of AI ≥ 0.32, while the ratios were significantly larger than 1 at the sites of AI ≤ 0.22. This observation suggests that the cycling of organic matter at sites of AI ≥ 0.32 significantly influences REE budget and transfer in soil, while abiotic processes (e.g., mineral dissolution, formation and translocation) play a more important role in controlling REE distribution at the site of AI ≤ 0.22. Our findings highlight a transition from abiotic to biotic control on rare earth elements in the soil along the large-scale climosequence. Moreover, we observed a significant correlation between AI and ratios of the sum of carbonate-bound and reducible REE contents to oxidizable REE contents ($R^2 = 0.59$, $P < 0.05$, Fig. 6) across the large-scale transect. The correlation indicated the importance of the biotic and abiotic processes on REE related to AI. The intertwined effects of abiotic and biotic processes on rare earth elements translocation within soils across the large-scale climatic transect can be broadly deconvoluted via the relation between geochemical parameters and climatic parameters, to reveal how REE cycling in soils would respond under global climate change, and provide a scientific basis of the sustainable development of the ecologically fragile areas.

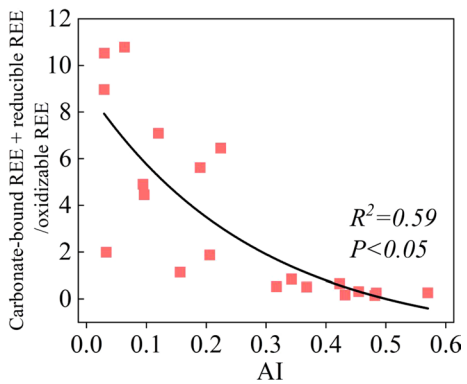


**Fig. 6** The correlation of the ratios of the sum of carbonate-bound and reducible REE content to oxidizable REE content (unless) against aridity index (AI) ($R^2 = 0.59$, $P < 0.05$)

### Normalized REE patterns of geochemical fractions in topsoils

Overall HREE depletions compared to MREE and LREE were observed in the UCC-normalized REE patterns of carbonate-bound ($La_N/Yb_N = 1.2–4.5$, $Gd_N/Yb_N = 1.9–3.8$) and reducible components ($La_N/Yb_N = 0.8–3.1$, $Gd_N/Yb_N = 1.7–2.4$). This depletion may arise from progressive enhanced complexation and solubility in soil solutions from LREE to HREE (Khorasanipour and Jafari 2018), thereby leading to disproportionately fractionation and loss of the three different groups of REE in topsoils. The signature of the HREE depletion may partly inherit from their parent rock, which is also seen in the residue fraction (Fig. 3d, Additional file 2: Table S4). In addition, fractionations between LREE and MEEE (represented by $La_N/Gd_N$) in carbonate-bounded and reducible components ($P < 0.01$, Additional file 1: Fig. S2) were positively correlated to the climatic factor of MAP. The shift from MREE enrichment ($La_N/Gd_N < 1.0$) to depletion ($La_N/Gd_N > 1.0$) relative to LREE suggest factors/properties other than complexation and solubility influence MREE affinity with carbonate and Fe–Mn (hydro)oxides, but not specifically identified in this study partly due to lack of kinematics data.

Moderate MREE enrichments ($Gd_N/Yb_N = 1.2–2.1$) compared to HREE were also observed in the UCC-normalized patterns of oxidizable fractions (Fig. 3c, Additional file 2: Table S4). Stronger complexation of MREE with convex carboxylic acids and high stability of organic matter complexes in soil may contribute to their enrichments in oxidizable fractions (Marsac et al. 2013; Zhang et al. 1998; Laveuf and Cornu 2009). A complementary moderate LREE depletions compared to HREE ($La_N/Yb_N = 0.5–0.9$, Additional file 2: Table S4) were observed in oxidizable fractions at arid sites (AI < 0.22, except for S02), reflecting negligible loss of REE to soil through leaching. In contrast, no pronounced LREE depletion or enrichment compared to HREE ($La_N/Yb_N = 0.8–1.2$) were found at semi-arid and dry sub-humid sites (AI > 0.3), suggesting no preferentially bound to organic matters under these environmental conditions.

Ce anomalies ($Ce/Ce^* = 0.9–1$) in bulk REE were close to 1; however, large negative Ce anomalies ($Ce/Ce^* = 0.3–0.9$) were shown in the carbonate-bound fractions (Fig. 3a, Additional file 2: Table S4). In soil solutions, the common $Ce^{3+}$ ion can be readily oxidized into $Ce^{4+}$ ion under oxidative conditions. The $Ce^{4+}$ ion may be subsequently absorbed on the insoluble particles, such as Fe/Mn (hydro)oxides and organic matter in topsoils (Laveuf & Cornu, 2009; Leybourne & Johannesson 2008).

This is also consistent with overall positive and complementary Ce anomalies in reducible ($Ce/Ce^* = 0.6–1.1$) and oxidizable fractions ($Ce/Ce^* = 0.7–1.2$). Note that Ce anomalies values ($Ce/Ce^* < 1.0$) in reducible and oxidizable fractions may reflect the loss in the open system of REE in topsoils to some extent.

Positive Eu anomalies were found in bulk REE ($Eu/Eu^* = 1–1.3$). The positive Eu anomalies were likely inherited from their parent rocks. Feldspar is known to contain fewer amounts of REE except for Eu (Compton et al. 2003), because $Eu^{2+}$ preferentially replaces $Ca^{2+}$ in feldspar, while all other rare earth elements are trivalent (except for Ce). Therefore, the consistently positive Eu anomalies ($Eu/Eu^* = 1.0–1.6$) in residue fractions likely reflected the presence of abundant plagioclase feldspar in these sites. The mineralogical compositions in soils verified the existence of feldspar (Additional file 2: Table S2). The moderate Eu positive anomalies also were observed in the carbonate-bound ($Eu/Eu^* = 0.9–1.9$) and oxidizable REE ($Eu/Eu^* = 0.7–1.2$) as shown in Fig. 3. The element of Eu is a valence variable element that could be reduced from $Eu^{3+}$ to $Eu^{2+}$. The $Eu^{2+}$ prefer to be sequestered into the extracting phase and convey to other layers or substances (Chang et al. 2016; Prudêncio et al. 2011). However, the overall negative Eu anomalies ($Eu/Eu^* = 0.6–1.1$) also were shown in the reducible fractions, which may be due to the incomplete extraction of hydroxylamine hydrochloride solution (Leybourne and Johannesson 2008).

#### REE exchange in soil depth-profiles

REE abundances in natural soils are generally controlled by their parent materials, intensities of weathering, and pedogenic processes. The REE behaviors in the soil depth-profile depend mostly on climatic factors and the local edaphic properties. In addition, root biolifting, soil animal activity, and soil water transport all together exert a complex influence on the distribution of REE (Stille et al. 2009; Vermeire et al. 2016; Wen et al. 2006). Specifically, the biogeochemical cycling of REE in soils can be viewed as mass transfer within different geochemical fractions and soil horizons or mass fluxes into and/or out of soils. Constraints on changes in the REE abundances and UCC-normalized REE patterns may provide critical clues to decipher in-soil processes and evaluate the states (e.g., fully open-system condition, semi closed-system condition and/or transient steady state) of the studied soil system.

As shown in Fig. 4, both absolute REE contents and proportions in geochemical fractions of soil depth profiles at respective sites of S03, S09, S13, and S19, varied in a wide range. However, the UCC normalized patterns in bulk REE and geochemical fractions (Fig. 5, Additional file 2: Table S5 and S7) were greatly similar features. These results suggested that REE was partitioned into the different geochemical fractions during pedogenesis and successive processes within soils, but no significant fractionations among the three groups of REE (LREE, MREE and HREE). Thus, the soil system studied here can be viewed at a transient steady state. Note that the inferred steady-state REE cycling does not imply REE contents in soils were constant over the course of soil formation and development, but imply the response time of REE due to addition/loss processes match the residence time of REE in soils. In the following discussion, only qualitative generalization can be drawn from the limited data set, mostly due to the paucity of in-situ soil, parent materials and water data in this study.

At the hyper-arid and arid sites of S03 and S09, proportions of carbonate-bound fractions were significantly higher than those at the semi-arid and dry sub-humid sites of S13 and S19 (Fig. 4). As shown in Fig. 4 and Additional file 2: Table S6, carbonate-bound REE abundances in the upper soil (0–40 cm) at the site of S03 (11.3–12.0 μg $g^{-1}$, 0–10, 10–20, and 20–40 cm) was significantly larger than the deeper soil (40–100 cm) (0.4–1.0 μg $g^{-1}$, 40–60 and 60–100 cm). The greater carbonate-bound fractions in the upper soil may be due to the upward transfer of REE from deeper soil by evaporation in arid sites soil (Khorasanipour and Jafari 2018). This also can be applied to interpret the observation of REE contents at different soil layers in reducible fractions at S03 (Fig. 4, Additional file 2: Table S6).

Another noticeable observation is REE contents in topsoils and oxidizable fractions were significantly greater than that in the underlying soil, as the aridity index increased (Fig. 4 and Additional file 2: Table S6). For example, REE abundances in oxidizable fractions at the site of S19 had shown progressively upward-increasing (from 16.3 to 63.0 μg $g^{-1}$, Fig. 4). This observation is consistent with the suggestion that organic matter would be the most important carrier of REE in soil depth profiles, while the Fe /Mn oxide and carbonate have minor contributions (Jin et al. 2017). Under wetter environments, plant productivity and microbial biomass may be enhanced, thereby promoting the production and preservation of organic matter in topsoils.

Besides the upward transfer of REE in the soil depth profiles, a downward transfer of complexations of Fe/Mn oxides and organic matter may occur. For example, REE contents in reducible fractions and oxidizable fractions slightly increased with the depth at the arid and semi-arid sites of S09 and S13 (Fig. 4, Additional file 2: Table S6). The observed trends may be related to the downward transfer of those REE geochemical complexes in the soil depth profiles, reflecting a minor contribution

of biological effects on the REE redistribution, but a major role of abiotic effects on REE mobility.

### Implications for sustainable development

Sustainable development is a key concept for our modern civilization and future prospects, which mainly concerns the harmonious development among humans, the economy and ecosystems on our planet. Evolution and development of all life, environments and our society on earth rely on the cycling of critical elements (such as C, N, S, O, P, Fe, Mo, Cu, Zn and REE) in a dynamically interconnected subsystem of the Earth (e.g., atmosphere–plant–soil subsystem). In this study, we provide a preliminary understanding of how REE in less-disturbed pristine soils fractionated and redistributed, and also provide a basic hypothesis of how REEs in soils respond to a large-scale climate gradient. Our results demonstrated that a significant portion of rare earth elements is labile that could circulate in the terrestrial ecosystem. Such results would help evaluate the positive and adverse impacts on plant growth with the increasing use of REE as agricultural fertilizers in human-impacted systems, and would be potentially beneficial to sustainably manage and mine REE in the terrestrial ecosystem for industry applications (Adeel et al. 2021; Chen et al. 2020; Dushyantha et al. 2020; Tripathee et al. 2016).

## Conclusions

Our data among the first to characterize REE distributions and behavior of bulk and geochemical fractions in soils and study the relationship between REE geochemistry and climatic factors along a large-scale climosequence in arid and semiarid grasslands of northern China. Similar upper-continental-crust (UCC) normalized REE patterns of bulk and respective geochemical components suggest that REE in soils may inherited from common parent materials. These results indicate a transition from geochemical to biotic control on soil REE cycling with decreasing aridity across a threshold of 0.2–0.3. Our findings highlight the importance of climate factors (e.g., MAT and MAP) and soil properties (e.g., organic carbon and clay contents) on elemental cycling and carry implications for sustainable development and ecosystem services. In addition, our results open up new opportunities to further study factors and processes that control the REE cycle in soils. These include: (1) studying mineral-scale selective adsorption and affinity of REE in soils; (2) performing extensive research on the REE cycle along toposequences and chronosequences from a wide range of climates; (3) developing non-steady state models by incorporation of soil properties (e.g., salinity and pH value) to trace REE mass balance in the rock–soil–plant system and quantify the role of underlying processes. Such studies will continue to improve our understanding of the ecosystem REE cycling across tempo-spatial scales under global environmental changes.

## Supplementary Information

The online version contains supplementary material available at https://doi.org/10.1186/s13717-022-00375-z.

**Additional file 1. Fig. S1.** Overview of the modified BCR sequential extraction method for REE in this study. **Fig. S2.** The relationships of the values of $La_N/Gd_N$ of carbonate-bound and reducible with mean annual precipitation ($R^2_{\text{carbonate-bound}} = 0.2$, $P < 0.05$; $R^2_{\text{reducible}} = 0.9$, $P < 0.01$).

**Additional file 2. Table S1.** The parameters and bulk REE concentrations (μg $g^{-1}$ soil) in topsoils (0–10 cm) along the transect. Locations of the sites (S01–S21) are plotted in Fig. 1. **Table S2.** The mineral composition (%) in topsoils (0–10 cm) along the transect. Locations of the sites (S01–S21) are plotted in Fig. 1. **Table S3.** The fractional and bulk REE concentrations (μg $g^{-1}$) in topsoils (0–10 cm) along the transect. Locations of the sites (S01–S21) are plotted in Fig. 1. **Table S4.** The REE geochemistry in different soil components (carbonate-bound, reducible, oxidizable, residue) in topsoils (0–10 cm) along the transect. Locations of the sites (S01–S21) are plotted in Fig. 1. **Table S5.** The parameters and REE concentrations (μg $g^{-1}$ soil) along the soil profile (0–10, 10–20, 20–40, 40–60, 60–100 cm) at selected sites (S03, aridity index (AI)=0.03; S09, AI=0.10; S13, AI=0.22; S19, AI=0.51). **Table S6.** The fractional and bulk REE concentrations (μg $g^{-1}$ soil) along the soil profile (0–10, 10–20, 20–40, 40–60, 60–100 cm) at selected sites (S03, aridity index (AI)=0.03; S09, AI=0.10; S13, AI=0.22; S19, AI=0.51). **Table S7.** The parameters of geochemical REE (carbonate-bound, reducible, oxidizable, residue) along the soil profile (0–10, 10–20, 20–40, 40–60, 60-100 cm) at selected sites (S03, aridity index (AI)=0.03; S09, AI=0.10; S13, AI=0.22; S19, AI=0.51).

#### Acknowledgements

We want to acknowledge Wenshuai Li and Xikai Wang for their helpful discussion about ICP-MS analysis and REE geochemistry extraction. This study was supported by Chinese Academy of Sciences (No. E01X0301), National Natural Science Foundation of China (Grant No. 41673005). Yi-Wen Cao gratefully acknowledges financial support from China Scholarship Council.

#### Authors' contributions

Y-WC: data curation; formal analysis; writing—original draft; and writing—review and editing. X-ML: conceptualization; methodology; and writing—review and editing. CW: investigation and writing—review and editing. EB: conceptualization, writing—review and editing, and supervision. NW: project administration, supervision, writing—review and editing, and funding acquisition. All authors read and approved the final manuscript.

#### Funding

This study was supported by Chinese Academy of Sciences (No. E01X0301), National Natural Science Foundation of China (Grant No. 41673005). Yi-Wen Cao gratefully acknowledges financial support from China Scholarship Council. Youth Innovation Promotion Association CAS to Chao Wang (2018231).

#### Availability of data and materials

All data generated or analyzed during this study are included in this published article and its supplementary information files.

## Declarations

#### Ethics approval and consent to participate

Not applicable.

#### Consent for publication

Not applicable. All authors agreed and approved the manuscript for publication in *Ecological Processes.*

**Competing interests**
The authors declare that they have no competing interests. The content is new and has not been published in any journal.

**Author details**
[1]CAS Key Laboratory of Forest Ecology and Management, Institute of Applied Ecology, Chinese Academy of Sciences, Shenyang 110016, China. [2]University of Chinese Academy of Sciences, Beijing 100049, China. [3]Department of Earth, Marine and Environmental Sciences, University of North Carolina-Chapel Hill, Chapel Hill, NC 27515, USA. [4]Key Laboratory of Geographical Processes and Ecological Security of Changbai Mountains, School of Geographical Sciences, Northeast Normal University, Changchun 130024, China. [5]Present Address: Institute of Deep-Sea Science and Engineering, Chinese Academy of Sciences, Sanya 572000, China.

Received: 25 January 2022 Accepted: 12 March 2022
Published online: 21 March 2022

**References**

Adeel M, Shakoor N, Ahmad MA, White JC, Jilani G, Rui Y (2021) Bioavailability and toxicity of nanoscale/bulk rare earth oxides in soil: physiological and ultrastructural alterations: Eisenia Fetida. Environ Sci Nano 8:1654–1666. https://doi.org/10.1039/d1en00116g

Andrade GRP, Cuadros J, Barbosa JMP, Vidal-Torrado P (2022) Clay minerals control rare earth elements (REE) fractionation in Brazilian mangrove soils. Catena 209:105855. https://doi.org/10.1016/j.catena.2021.105855

Balaram V (2019) Rare earth elements: a review of applications, occurrence, exploration, analysis, recycling, and environmental impact. Geosci Front 10:1285–1303. https://doi.org/10.1016/j.gsf.2018.12.005

Brito P, Caetano M, Martins MD, Caçador I (2021) Effects of salt marsh plants on mobility and bioavailability of REE in estuarine sediments. Sci Total Environ 759:144314. https://doi.org/10.1016/j.scitotenv.2020.144314

Cao X, Wang X, Zhao G (2000) Assessment of the bioavailability of rare earth elements in soils by chemical fractionation and multiple regression analysis. Chemosphere 40:23–28. https://doi.org/10.1016/S0045-6535(99)00225-8

Cao X, Chen Y, Wang X, Deng X (2001) Effects of redox potential and pH value on the release of rare earth elements from soil. Chemosphere 44:655–661. https://doi.org/10.1016/S0045-6535(00)00492-6

Chang C, Li F, Liu C, Gao J, Tong H, Chen M (2016) Fractionation characteristics of rare earth elements (REEs) linked with secondary Fe, Mn, and Al minerals in soils. Acta Geochim 35:329–339. https://doi.org/10.1007/s11631-016-0119-1

Chapela M, Buss HL, Pett-ridge JC (2018) The effects of lithology on trace element and REE behavior during tropical weathering. Chem Geol 500:88–102. https://doi.org/10.1016/j.chemgeo.2018.09.024

Chen J, Yang R (2010) Analysis on REE geochemical characteristics of three types of REE-rich soil in Guizhou Province, China. J Rare Earths 28:517–522. https://doi.org/10.1016/S1002-0721(10)60271-2

Chen LM, Zhang GL, Jin ZD (2014) Rare earth elements of a 1000-year paddy soil chronosequence: Implications for sediment provenances, parent material uniformity and pedological changes. Geoderma 230–231:274–279. https://doi.org/10.1016/j.geoderma.2014.03.023

Chen H, Chen Z, Chen Z, Ou X, Chen J (2020) Calculation of toxicity coefficient of potential ecological risk assessment of rare earth elements. Bull Environ Contam Toxicol 104:582–587. https://doi.org/10.1007/s00128-020-02840-x

Compton JS, White RA, Smith M (2003) Rare earth element behavior in soils and salt pan sediments of a semi-arid granitic terrain in the Western Cape, South Africa. Chem Geol 201:239–255. https://doi.org/10.1016/S0009-2541(03)00239-0

Davranche M, Grybos M, Gruau G, Pédrot M, Dia A, Marsac R (2011) Rare earth element patterns: a tool for identifying trace metal sources during wetland soil reduction. Chem Geol 284:127–137. https://doi.org/10.1016/j.chemgeo.2011.02.014

Du Laing G, Rinklebe J, Vandecasteele B, Meers E, Tack FMG (2009) Trace metal behaviour in estuarine and riverine floodplain soils and sediments: a review. Sci Total Environ 407:3972–3985. https://doi.org/10.1016/j.scitotenv.2008.07.025

Dushyantha N, Batapola N, Ilankoon IMSK, Rohitha S, Premasiri R, Abeysinghe B, Ratnayake N, Dissanayake K (2020) The story of rare earth elements (REEs): Occurrences, global distribution, genesis, geology, mineralogy and global production. Ore Geol Rev 122:103521. https://doi.org/10.1016/j.oregeorev.2020.103521

FAO (1993) Global and national soils and terrain digital databases (SOTER): Procedures manual. In: World Soil Resources Reports, edited by Food and Agriculture Organization of the United Nations, Rome, Italy

FAO (2014) Global and national soils and terrain digital databases (SOTER): Procedures manual. In: World Soil Resources Reports, edited by Food and Agriculture Organization of the United Nations, Rome, Italy

Feng J, Turner BL, Lü X, Chen Z, Wei K, Tian J, Wang C, Luo W, Chen L (2016) Phosphorus transformations along a large-scale climosequence in arid and semiarid grasslands of northern China. Global Biogeochem Cycles 30:1264–1275. https://doi.org/10.1002/2015GB005331

Ferrat M, Weiss DJ, Strekopytov S, Dong S, Chen H, Najorka J, Sun Y, Gupta S, Tada R, Sinha R (2011) Improved provenance tracing of Asian dust sources using rare earth elements and selected trace elements for palaeomonsoon studies on the eastern Tibetan Plateau. Geochim Cosmochim Acta 75:6374–6399. https://doi.org/10.1016/j.gca.2011.08.025

Filgueiras AV, Lavilla I, Bendicho C (2002) Chemical sequential extraction for metal partitioning in environmental solid samples. J Environ Monit 4:823–857. https://doi.org/10.1039/b207574c

García-Miragaya J, Sosa AM (1994) Trace metals in Valencia lake (Venezuela) sediments. Water Air Soil Pollut 77:141–150. https://doi.org/10.1007/BF00483054

Guénet H, Demangeat E, Davranche M, Vantelon D, Pierson-Wickmann AC, Jardé E, Bouhnik-Le Coz M, Lotfi E, Dia A, Jestin J (2018) Experimental evidence of REE size fraction redistribution during redox variation in wetland soil. Sci Total Environ 631–632:580–588. https://doi.org/10.1016/j.scitotenv.2018.03.005

Hu Z, Haneklaus S, Sparovek G, Schnug E (2006) Rare earth elements in soils. Commun Soil Sci Plant Anal 37:1381–1420. https://doi.org/10.1080/00103620600628680

Humphries M (2010) Rare earth elements: the global supply chain. Diane Publishing. https://doi.org/10.1002/2016GC006659.Received

Jin L, Ma L, Dere A, White T, Mathur R, Brantley SL (2017) REE mobility and fractionation during shale weathering along a climate gradient. Chem Geol 466:352–379. https://doi.org/10.1016/j.chemgeo.2017.06.024

Khorasanipour M, Jafari Z (2018) Environmental geochemistry of rare earth elements in Cu-porphyry mine tailings in the semiarid climate conditions of Sarcheshmeh mine in southeastern Iran. Chem Geol 477:58–72. https://doi.org/10.1016/j.chemgeo.2017.12.005

Kumari A, Panda R, Jha MK, Kumar JR, Lee JY (2015) Process development to recover rare earth metals from monazite mineral: a review. Miner Eng 79:102–115. https://doi.org/10.1016/j.mineng.2015.05.003

Laveuf C, Cornu S (2009) A review on the potentiality of Rare Earth Elements to trace pedogenetic processes. Geoderma 154:1–12. https://doi.org/10.1016/j.geoderma.2009.10.002

Laveuf C, Cornu S, Guilherme LRG, Guerin A, Juillot F (2012) The impact of redox conditions on the rare earth element signature of redoximorphic features in a soil sequence developed from limestone. Geoderma 170:25–38. https://doi.org/10.1016/j.geoderma.2011.10.014

Leybourne MI, Johannesson KH (2008) Rare earth elements (REE) and yttrium in stream waters, stream sediments, and Fe-Mn oxyhydroxides: fractionation, speciation, and controls over REE + Y patterns in the surface environment. Geochim Cosmochim Acta 72:5962–5983. https://doi.org/10.1016/j.gca.2008.09.022

Li W, Liu XM, Godfrey LV (2019) Optimisation of lithium chromatography for isotopic analysis in geological reference materials by MC-ICP-MS. Geostand Geoanal Res 43:261–276. https://doi.org/10.1111/ggr.12254

Li W, Liu XM, Chadwick OA (2020) Lithium isotope behavior in Hawaiian regoliths: soil-atmosphere-biosphere exchanges. Geochim Cosmochim Acta 285:175–192. https://doi.org/10.1016/j.gca.2020.07.012

Liu XM, Hardisty DS, Lyons TW, Swart PK (2019) Evaluating the fidelity of the cerium paleoredox tracer during variable carbonate diagenesis on the Great Bahamas Bank. Geochim Cosmochim Acta 248:25–42. https://doi.org/10.1016/j.gca.2018.12.028

Liu C, Liu WS, van der Ent A, Morel JL, Zheng HX, Wang GB, Tang YT, Qiu RL (2021a) Simultaneous hyperaccumulation of rare earth elements, manganese and aluminum in *Phytolacca americana* in response to soil

properties. Chemosphere 282:131096. https://doi.org/10.1016/j.chemosphere.2021.131096
Liu H, Guo H, Pourret O, Wang Z, Sun Z, Zhang W, Liu M (2021b) Distribution of rare earth elements in sediments of the North China Plain: A probe of sedimentation process. Appl Geochem 134:105089. https://doi.org/10.1016/j.apgeochem.2021.105089
Liu C, Liu WS, Huot H, Guo MN, Zhu SC, Zheng HX, Morel JL, Tang YT, Qiu RL (2022) Biogeochemical cycles of nutrients, rare earth elements (REEs) and Al in soil-plant system in ion-adsorption REE mine tailings remediated with amendment and ramie (*Boehmeria nivea* L.). Sci Total Environ 809:152075. https://doi.org/10.1016/j.scitotenv.2021.152075
Luo W, Dijkstra FA, Bai E, Feng J, Lü XT, Wang C, Wu H, Li MH, Han X, Jiang Y (2016a) A threshold reveals decoupled relationship of sulfur with carbon and nitrogen in soils across arid and semi-arid grasslands in northern China. Biogeochemistry 127:141–153. https://doi.org/10.1007/s10533-015-0174-4
Luo W, Sardans J, Dijkstra FA, Peñuelas J, Lü XT, Wu H, Li MH, Bai E, Wang Z, Han X, Jiang Y (2016b) Thresholds in decoupled soil-plant elements under changing climatic conditions. Plant Soil 409:159–173. https://doi.org/10.1007/s11104-016-2955-5
Marsac R, Davranche M, Gruau G, Dia A, Pédrot M, Le Coz-Bouhnik M, Briant N (2013) Effects of Fe competition on REE binding to humic acid: Origin of REE pattern variability in organic waters. Chem Geol 342:119–127. https://doi.org/10.1016/j.chemgeo.2013.01.020
Miao L, Xu R, Ma Y, Zhu Z, Wang J, Cai R, Chen Y (2008) Geochemistry and biogeochemistry of rare earth elements in a surface environment (soil and plant) in South China. Environ Geol 56:225–235. https://doi.org/10.1007/s00254-007-1157-0
Middleton N, Thomas D (1997) World Atlas of Desertification. Edward Arnold, London
Migaszewski ZM, Gałuszka A (2015) The characteristics, occurrence, and geochemical behavior of rare earth elements in the environment: a review. Crit Rev Environ Sci Technol 45:429–471. https://doi.org/10.1080/10643389.2013.866622
Mihajlovic J, Rinklebe J (2018) Rare earth elements in German soils—a review. Chemosphere 205:514–523. https://doi.org/10.1016/j.chemosphere.2018.04.059
Mihajlovic J, Giani L, Stärk HJ, Rinklebe J (2014) Concentrations and geochemical fractions of rare earth elements in two different marsh soil profiles at the North Sea, Germany. J Soils Sediments 14:1417–1433. https://doi.org/10.1007/s11368-014-0895-3
Mihajlovic J, Bauriegel A, Stärk HJ, Roßkopf N, Zeitz J, Milbert G, Rinklebe J (2019) Rare earth elements in soil profiles of various ecosystems across Germany. Appl Geochem 102:197–217. https://doi.org/10.1016/j.apgeochem.2019.02.002
Mittermüller M, Saatz J, Daus B (2016) A sequential extraction procedure to evaluate the mobilization behavior of rare earth elements in soils and tailings materials. Chemosphere 147:155–162. https://doi.org/10.1016/j.chemosphere.2015.12.101
Pang X, Li D, Peng A (2001) Application of rare-earth elements in the agriculture of china and its environmental behavior in soil. J Soils Sediments 1:124–129. https://doi.org/10.1065/iss2001.05.013
Pédrot M, Dia A, Davranche M, Gruau G (2015) Upper soil horizons control the rare earth element patterns in shallow groundwater. Geoderma 239:84–96. https://doi.org/10.1016/j.geoderma.2014.09.023
Polyakov VO, Nearing MA (2003) Sediment transport in rill flow under deposition and detachment conditions. Catena 51:33–43. https://doi.org/10.1016/S0341-8162(02)00090-5
Pourret O, Davranche M, Gruau G, Dia A (2007) Rare earth elements complexation with humic acid. Chem Geol 243:128–141. https://doi.org/10.1016/J.CHEMGEO.2007.05.018
Prudêncio MI, Dias MI, Waerenborgh JC, Ruiz F, Trindade MJ, Abad M, Marques R, Gouveia MA (2011) Rare earth and other trace and major elemental distribution in a pedogenic calcrete profile (Slimene, NE Tunisia). Catena 87:147–156. https://doi.org/10.1016/j.catena.2011.05.018
Rankin PC, Childs CW (1976) Rare-earth elements in iron-manganese concretions from some New Zealand soils. Chem Geol 18:55–64. https://doi.org/10.1016/0009-2541(76)90061-9
Rauret G, López-Sánchez JF, Sahuquillo A, Rubio R, Davidson C, Ure A, Quevauviller P (1999) Improvement of the BCR three step sequential extraction procedure prior to the certification of new sediment and soil reference materials. J Environ Monit 1:57–61. https://doi.org/10.1039/a807854h
Shatrova YN, Dzhenloda RK, Fedyunina NN, Karandashev VK, Fedotov PS (2021) A Comparative study of methods of the dynamic fractionation of rare earth elements in soils. J Anal Chem 76:1144–1152. https://doi.org/10.1134/S1061934821100105
Šmuc NR, Dolenec T, Serafimovski T, Dolenec M, Vrhovnik P (2012) Geochemical characteristics of rare earth elements (REEs) in the paddy soil and rice (*Oryza sativa* L.) system of Kočani Field, Republic of Macedonia. Geoderma 183–184:1–11. https://doi.org/10.1016/j.geoderma.2012.03.009
Stille P, Pierret MC, Steinmann M, Chabaux F, Boutin R, Aubert D, Pourcelot L, Morvan G (2009) Impact of atmospheric deposition, biogeochemical cycling and water-mineral interaction on REE fractionation in acidic surface soils and soil water (the Strengbach case). Chem Geol 264:173–186. https://doi.org/10.1016/j.chemgeo.2009.03.005
Sukitprapanon TS, Suddhiprakarn A, Kheoruenromne I, Gilkes RJ (2019) Rare earth elements in acid sulfate soils under long-term paddy rice cultivation in Thailand. Geoderma Reg 17:e00216. https://doi.org/10.1016/j.geodrs.2019.e00216
Taylor SR, McLennan SM (1985) The continental crust: its composition and evolution. Blackwell, Oxford
Taylor SR, McLennan S, Armstrong R, Tarney J (1981) The composition and evolution of the continental crust : rare earth element evidence from sedimentary rocks. Phil Trans R Soc Lond A 301:381–399. https://doi.org/10.1098/rsta.1981.0119
Tripathee L, Kang S, Rupakheti D, Zhang Q, Bajracharya RM, Sharma CM, Huang J, Gyawali A, Paudyal R, Sillanpää M (2016) Spatial distribution, sources and risk assessment of potentially toxic trace elements and rare earth elements in soils of the Langtang Himalaya, Nepal. Environ Earth Sci 75:1332. https://doi.org/10.1007/s12665-016-6140-1
Tyler G (2004) Rare earth elements in soil and plant systems—a review. Plant Soil 267:191–206. https://doi.org/10.1007/s11104-005-4888-2
Vermeire ML, Cornu S, Fekiacova Z, Detienne M, Delvaux B, Cornélis JT (2016) Rare earth elements dynamics along pedogenesis in a chronosequence of podzolic soils. Chem Geol 446:163–174. https://doi.org/10.1016/j.chemgeo.2016.06.008
Wang C, Wang X, Liu D, Wu H, Lü X, Fang Y, Cheng W, Luo W, Jiang P, Shi J, Yin H, Zhou J, Han X, Bai E (2014) Aridity threshold in controlling ecosystem nitrogen cycling in arid and semi-arid grasslands. Nat Commun 5:4799. https://doi.org/10.1038/ncomms5799
Wen B, Liu Y, Hu XY, Shan XQ (2006) Effect of earthworms (Eisenia fetida) on the fractionation and bioavailability of rare earth elements in nine Chinese soils. Chemosphere 63:1179–1186. https://doi.org/10.1016/j.chemosphere.2005.09.002
Zhang Y, Gao X (2015) Rare earth elements in surface sediments of a marine coast under heavy anthropogenic influence: the Bohai Bay, China. Estuar Coast Shelf Sci 164:86–93. https://doi.org/10.1016/j.ecss.2015.07.017
Zhang C, Wang L, Zhang S, Li X (1998) Geochemistry of rare earth elements in the mainstream of the Yangtze River, China. Appl Geochem 13:451–462. https://doi.org/10.1016/S0883-2927(97)00079-6

## Publisher's Note